Bull Volcanol (2009) 71:1057–1075
DOI 10.1007/s00445-009-0286-6

RESEARCH ARTICLE

Testing the suitability of frictional behaviour for pyroclastic flow simulation by comparison with a well-constrained eruption at Tungurahua volcano (Ecuador)

Karim Kelfoun · Pablo Samaniego · Pablo Palacios · Diego Barba

Received: 8 April 2008 / Accepted: 24 April 2009 / Published online: 16 May 2009

Abstract We use a well-monitored eruption of Tungurahua volcano to test the validity of the frictional behaviour, also called Mohr–Coulomb, which is generally used in geophysical flow modelling. We show that the frictional law is not appropriate for the simulation of pyroclastic flows at Tungurahua. With this law, the longitudinal shape of the simulated flows is a thin wedge of material progressively passing, over several hundreds of metres, from an unrealistic thickness at the front (<<1 mm) to some tens of centimetres. Simulated deposits form piles which accumulate at the foot of the volcano and are more similar to sand piles than natural pyroclastic deposits. Finally, flows simulated with a frictional rheology are not channelised by the drainage system, but affect all the flanks of the volcano. In addition, their velocity can exceed 150 m s^{-1}, allowing pyroclastic flows to cross interfluves at bends in the valley, affecting areas that would not have been affected in reality and leaving clear downstream areas that would be covered in reality. Instead, a simple empirical law, a constant retarding stress (i.e. a yield strength), involving only one free parameter, appears to be much better adapted for modelling pyroclastic flows. A similar conclusion was drawn for the Socompa debris avalanche simulation (Kelfoun and Druitt, J Geophys Res 110:B12202, 2005).

Keywords Pyroclastic flows · Numerical simulation · Rheology · Tungurahua

Editorial responsibility: J.C. Phillips

Electronic supplementary material The online version of this article (doi:10.1007/s00445-009-0286-6) contains supplementary material, which is available to authorized users.

K. Kelfoun
IRD—Instituto Geofisico, Escuela Politecnica Nacional Casilla, 1701-2759 Quito, Ecuador

K. Kelfoun (✉)
Laboratoire Magmas et Volcans, Université Blaise Pascal, CNRS, IRD–OPGC,
5 rue Kessler,
63038 Clermont-Ferrand, France
e-mail: k.kelfoun@opgc.univ-bpclermont.fr
URL: http://wwwobs.univ-bpclermont.fr/lmv/pperm/kelfoun_k

P. Samaniego · P. Palacios · D. Barba
Instituto Geofisico, Escuela Politecnica Nacional Casilla, 1701-2759 Quito, Ecuador

Introduction

Numerical simulations of pyroclastic flows are increasingly being used for hazard assessment on volcanoes and will be essential for future hazard mitigation. A potential problem of such an approach, however, is that the rheological behaviour of such flows is very complex. Several approaches have improved our understanding of these kind of flows by trying to describe, physically, the complexities of pyroclastic density currents (e.g. Burgisser and Bergantz 2002; Neri et al. 2003; Dartevelle 2004). At present, however, this complexity is too high to be fully described. Dense pyroclastic flows, the subject of this paper, are formed by blocks and ash that vibrate, collide, rub together, break and interact by electrostatic forces during transport. Complex interactions also exist between particles and magmatic and atmospheric gases. As we do not understand all the complexities of these interactions at a microscopic level, we cannot simulate them accurately and we have to use simplified rheological laws that fit the general behaviour. Initially, however, we should ensure that they reproduce the first order features of the natural phenomenon.

Existing models of dense pyroclastic flows generally start with the assumption that frictional behaviour is dominant in their rheology and that it plays the major role in deposit formation. This behaviour seems logical because it is exhibited by pyroclastic flow deposits or, more commonly, by sand at rest. This behaviour is inferred from the energy line and energy cone models initially used for rock avalanches (Heim 1882; Hsü 1975), then subsequently for pyroclastic flows (Sheridan 1979). It also approximates well the behaviour of sand flows in the laboratory (e.g. Savage and Hutter 1989; Gray et al. 2003; Pouliquen and Forterre 2002). Patra et al. (2005, 2006) simulate the pyroclastic flows of Colima volcano with the code Titan2D, using a frictional model with two friction angles. Other authors consider the retarding stress as a combination of a frictional stress plus a viscous and/or a turbulent stress: McEwen and Malin (1989) use a kinetic approach to simulate pyroclastic flows on Mt St. Helens; Wadge et al. (1998) and Saucedo et al. (2005) use the same approach to simulate dense flows on Soufrière Hill and Colima volcano, respectively.

The simplest form of the frictional model, also known as Mohr–Coulomb model, states that the resistive shear stress τ_r is a function of both the normal stress σ and the friction angle: $\tau_r=\sigma\tan\varphi$. The frictional stress is thus rate independent. A block with a frictional behaviour which is subjected to both a normal (σ) and a shear stress (τ_d) stays at rest whilst $\tau_d\leq\sigma\tan\varphi$. When the shear stress exceeds the threshold ($\tau_d>\sigma\tan\varphi$), the block accelerates. A block at rest on a slope α is submitted to a driving stress $\tau_d=\rho gh\sin\alpha$ and a retarding stress $\tau_r=\sigma\tan\varphi=\rho gh\cos\alpha\tan\varphi$, where ρ, h and g are respectively the density of the block, its thickness and gravity. It thus begins to slide when the driving stress exceeds the retarding stress $\tau_d>\tau_r$, i.e. when the slope exceeds the friction angle, $\alpha>\varphi$. Note that for the following, this threshold is independent of the thickness of the block. A frictional granular medium at rest exhibits a more complex behaviour than a block due to the additional stress of the pressure gradient. The angle of repose of a sand pile, for example, whose behaviour is frictional, corresponds to its angle of friction. A frictional flow exhibits a much more complex behaviour: It will begin to flow when its surface angle (from the horizontal) exceeds the angle of friction. However, once in movement, its surface angle can be lower or higher than the static value according to slope variations and to inertia.

The following key questions must be addressed before using this behaviour for hazard assessment: Is it realistic to consider pyroclastic flows as mainly frictional and is this behaviour compatible with field observations of their geometry, their relatively low velocity (generally <40 m s^{-1}) and their high mobility?

Tungurahua volcano (Ecuador) erupted in July and August 2006 and pyroclastic flows swept along the west flank of the volcano. The eruption was observed, described and monitored by the staff of the *Instituto Geofisico* of the *Escuela Politécnica Nacional* (IG-EPN), Quito. Based on their data, it is possible to reconstruct the conditions of pyroclastic flow formation, transport and emplacement. Eruptions of Tungurahua are a very interesting case to test the validity of the rheological models used for pyroclastic flow simulations and to answer the fundamental question of the adequacy of the frictional model.

The 2006 eruptions of Tungurahua volcano

General description of Tungurahua

Tungurahua volcano (5,023 m asl, 1°28′ S, 78°27′ W) is a steep-sided andesitic stratovolcano, located in central Ecuador, ranking as one of the most active volcanoes of the Northern Andes. During historical times, Tungurahua experienced important (VEI≥3) pyroclastic flow-forming eruptions in AD 1640–1641, 1773, 1886 and 1916–1918 (Hall et al. 1999; Le Pennec et al. 2008). The current eruptive episode began in 1999 and is still ongoing today (January 2009). Periods of low-to-moderate explosive activity occurred in November–December 1999, August 2001, September 2002 and October–November 2003. These periods were characterised by Strombolian activity, canon-like explosions and light-to-moderate regional ash fallouts. Periods of quiescence have also been observed, the most notable being from February to December 2005.

At the beginning of April 2006, IG-EPN scientists detected some deep long period seismic events (5–15 km depth) that preceded a change in the degassing pattern of the volcano (beginning of May), which was followed by an important deformation in the upper part of the cone (end of May). From the beginning of July, seismic activity increased dramatically and culminated with the 14th July (VEI 2) and 16–17th August 2006 (VEI 3) eruptions (Samaniego et al. 2007; Mothes et al. 2007; Hall et al. 2007). For the first time since the beginning of this eruptive cycle, Tungurahua volcano produced pyroclastic flows which swept over the western half of the cone, as well as giving rise to eruption columns greater than 16 km in height.

The voluminous deposits of the 16th–17th August eruption covered the July 14th deposits and the August eruption was studied in more detail and better monitored. We have thus chosen this eruption to test pyroclastic flow modelling.

Chronology of the 16–17th August eruption

Eruptive activity increased from the morning of August 16th. At 1430 hours (local time = GMT-5), eruptive activity was characterised by a vigorous and continuous ash and

vapour emission, reaching 2–3 km above the crater. The first small pyroclastic flow occurred around 1700 hours and descended down the NW flank, in the Cusua and Chontapamba gullies (Fig. 1). During the next few hours, the eruptive activity increased progressively. It was characterised by an almost continuous lava fountain reaching up to 300 m high, associated with a 3–4-km-high eruption column. Before 2100 hours, other small-volume pyroclastic flows occurred in the Cusua, Juive Grande and Vazcún valleys (Fig. 1). Other sporadic, but probably longer, pyroclastic flows were generated at 2114, 2126, 2143 and 2208 hours, related to explosions and/or an increase of the lava fountaining. Between 2200 and 0000 hours, other pyroclastic flows descended the Cusua–Bilbao area on the northwestern flank and the Juive Grande and Vazcun valleys on the northern flank.

The paroxysmal phase began at about 0015 hours and lasted around 40 min. Eruptive activity was characterised by a powerful lava fountain up to 1,000 m above the crater, a >16-km-high eruption column, and the quasi contemporaneous generation of the most voluminous pyroclastic flows, which descended via several quebradas on the N, NW, W and SW flanks (Vazcun, Juive Grande, Mandur, La Hacienda, Cusua, Achupashal, La Pirámide, Bilbao, Pingullo, Motilones, Chontapamba, de Romero, Ingapirca, Rea, Confesionario, Choglontus and Mapayacu). During this paroxysmal phase, the generation of pyroclastic flows was quasicontinuous as reported by inhabitants of the SW flank of the cone who remained in the Choglontus area (Fig. 1). The flows reached lengths of up to 8.5 km after a descent of 2,600–3,000 m from the summit crater. The pyroclastic flows of the Rea, Romero and Chontapamba formed deltas in the Rio Chambo valley, which was dammed for several hours after the eruption. The Mapayacu pyroclastic flows also dammed the Puela River.

No pyroclastic flow was witnessed on the eastern flank of the cone and no deposits were observed in this region during our helicopter survey. After the paroxysmal phase, both the

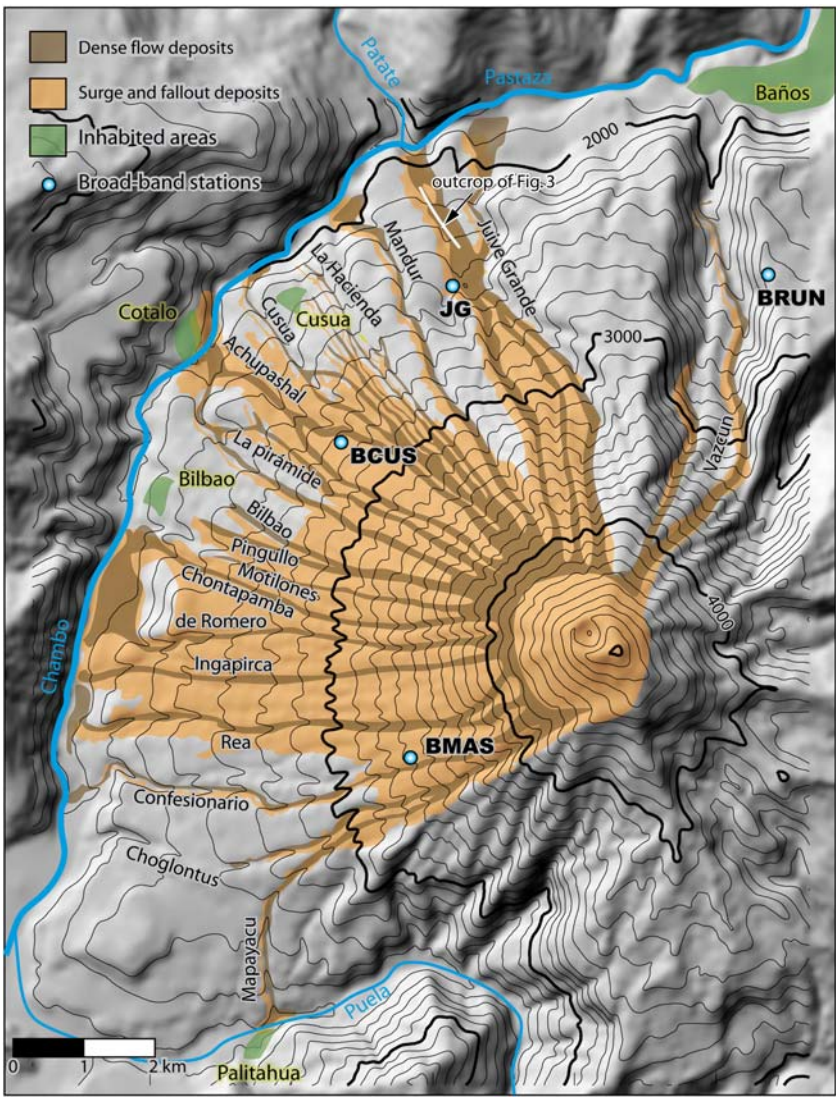

Fig. 1 Map of deposits of the August 2006 eruption of Tungurahua. Dense flow deposits are restricted to the drainage channels and are absent on the eastern flank as on steepest slopes of the summit cone. Seismic stations are *Brun* Runtun, *JG* Juive Grande, *Bcus* Cusua, *Bmas* Mason

seismic and the volcanic activity rapidly decreased and no further pyroclastic flows were emitted. On the afternoon of August 17th, IG-EPN thermal images of the NW flank confirmed the effusion of a voluminous blocky lava flow which was emitted some hours after the paroxysmal phase and which stopped at an elevation of 2,700 m asl (Fig. 2).

Description of deposits

Lithic-rich pyroclastic flow deposits are composed of juvenile, non- or poorly vesiculated blocks, associated cauliflower bombs and scoriae and accidental blocks. Their ratios of dense/vesiculate and juvenile/accidental components vary according to the unit and the valley studied. In Mapayacu, for example, accidentals represent more than 50% of the block facies. The more recent unit in Achupashal contains a high concentration of scoriae and bread crust bombs reaching more than 50 cm in diameter.

At least three distinct flow units were observed after the eruption, at the surface of the deposits, in the lower part (about 2,100 m asl) of the Juive Grande area (Hall et al. 2007), as well as in the Vazcún valley and most gullies on the western flank. Today (January 2009), incipient erosion of these deposits allows us to observe the different units and the internal structure of these pyroclastic flows (Fig. 3a, b). A maximum number of six distinct units can be observed in cross section, although the total number of units is probably even greater, since not all the units occur in each observed section. Each unit, which presents a well-defined front (Fig. 3c), is approximately 1 m thick on slopes <5°, becoming thinner on steeper slopes. It is difficult to quantify the relationship between thickness and slope because the thickness is also governed by changes in valley width. Thus, if the cross section of the deposit is located above the drainage channel, the true deposit thickness is exposed, whereas at the valley margins, the real thickness is underestimated. What is clear, however, from field observations as well as from the thermal image taken after the eruption (Fig. 2) is that few (or no) deposits can form on slopes greater than 25–30° and, which is important for validation of the model, that deposits are present where the slope is less than 25° (beneath 3,800 m asl), their thickness increasing as the slope decreases.

The total volume of the eruptive products, including ashes, has been estimated at more than $20\times10^6 m^3$. The overall volume of dense pyroclastic flow deposits is in the order of $5–10\times10^6 m^3$ (Hall et al. 2007). Due to the shape of the crater, whose NW border has a lower altitude, the deposits are more voluminous in the northwestern area (Achupashal, Cusua) than in the north and southwest drainage areas.

Ash cloud surges accompanied dense flows. Above 3,000 m asl, surges were able to leave the valleys, blowing down trees and creating several decimetre-thick ash deposits up to a distance of a hundred metres from the valley drainages. Below this height, trees were generally only knocked over on the convex sides of the valleys and only up to a distance of a few metres. Along the north and west/southwest drainage areas, there was very little damage to trees on the concave sides of the valleys even at the contact of dense flow deposits. Surge deposits were mainly observed in the northwest part (i.e. the central part) of the damaged area, facing the lowest point of the crater. Metre-thick surge deposits were observed all around the Achupashal valley (Fig. 1), forming ashy dunes with a typical anti-dune morphology. However, even here, trees were only swept down up to several tens of metres from the drainage channels covered by dense flows.

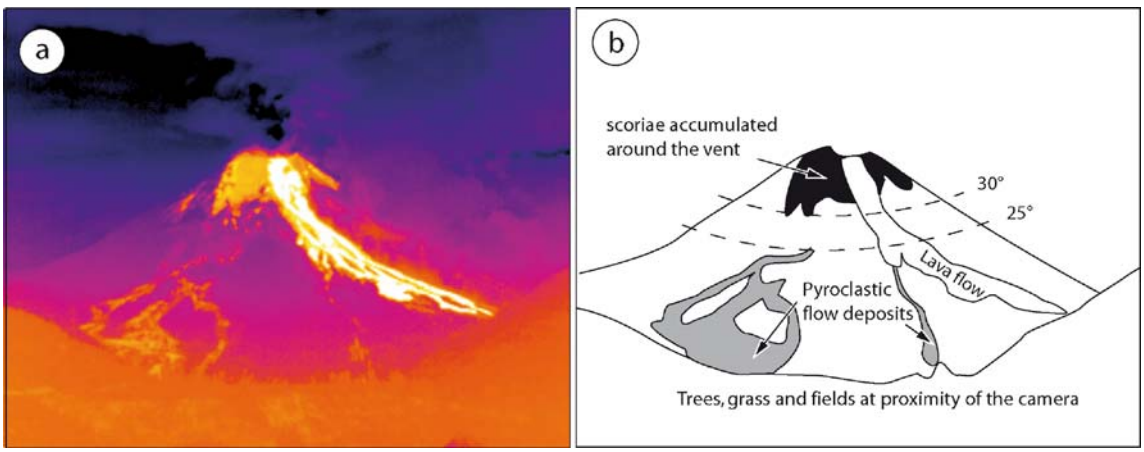

Fig. 2 **a** Thermal infrared image of August pyroclastic flows of Tungurahua and **b** sketch of the image. Note pyroclastic flow deposits on the lower slopes (between 0° and 25–30°, indicated on the *figure*) and scorias accumulated around the crater. The *white area* corresponds to a lava flow that followed pyroclastic flow emplacement. Courtesy of Santiago Arellano, IG-EPN

Fig. 3 **a** Erosion of pyroclastic deposits along Juive Grande (location on Fig. 1, *white line*). The 2008 units lies over older pyroclastic and lahar deposits. **b** Close up of pyroclastic units (*white frame* on **a**). The base of the 2008 flows is well marked by vegetation and objects (plastics, fence wires etc.). Three units, delimited by the *coloured arrows*, can be observed on the image. This kind of outcrop enables the number of units, their thickness and their variation of thickness according to the slope to be estimated. **c** A frontal lobe of the August pyroclastic deposits in Juive Grande

Seismic data

Broad band seismometers were installed around Tungurahua following a cooperative project between IG-EPN and Japan International Cooperation Agency (Kumagai et al. 2007) to monitor volcanic activity and forecast eruptions. Seismometers sample 50 data per second and are able to record frequencies from 1 to 25 Hz. During the crisis, they also recorded signals generated by vulcanian explosions and pyroclastic flows and are a powerful tool to confirm and quantify the emplacement of these flows. To exemplify this, we will focus on seismic signals recorded between 2100 and 2300 hours at Cusua station (located on the NW flank at 4.5 km from the crater, Bcus; Fig. 1). In this record, we observe several high-amplitude short duration (about 30 s) signals (at 2114, 2143 and 2208 hours, local time), which were followed by long coda signals with smaller amplitude (Fig. 4).

The high-amplitude signals were interpreted as explosive events, given that they were detected at nearly the same time by all the seismic stations according to their position relative to the crater. They are characterised by a frequency ranging across the whole spectrum (1 to 25 Hz), with a dominant frequency of 2–3 Hz (Fig. 4b).

The following and longer signals increased in amplitude for 150 s before diminishing. The amplitude increase is associated with an increase in the distribution of detected frequencies from <10 to 20 Hz (Fig. 4). Four observations show that these signals were generated by pyroclastic flows. Firstly, this signal cannot be correlated between the different stations although the recorded amplitudes are strong. The phenomenon that generated it must thus be local. Secondly, the Runtun seismic station, located at the margin of the area affected by the flows (about 600 m from the channel bottom), measured only a very weak increase in amplitude during the paroxysmal phase (Fig. 5). Since this station was able to record explosions at the crater, like the other stations, the lack of increased signal here confirms that the high frequency source recorded by the other stations in the affected area was local. Thirdly, the transmission systems of the stations located in the affected area were destroyed during the paroxysm. The time of destruction in Cusua (2126 hours) corresponds exactly to the arrival of pyroclastic flows. Another station (Juive Grande, not shown) recorded a very strong signal of this type (the strongest it recorded) just before it was destroyed at 0025 hours. Transmission at Mason, a little bit further from the valley, was interrupted at 0049 hours by ash deposits from pyroclastic flows which covered solar panels and antennae. Finally, visual observations confirm that these signals were associated with pyroclastic flow emplacement.

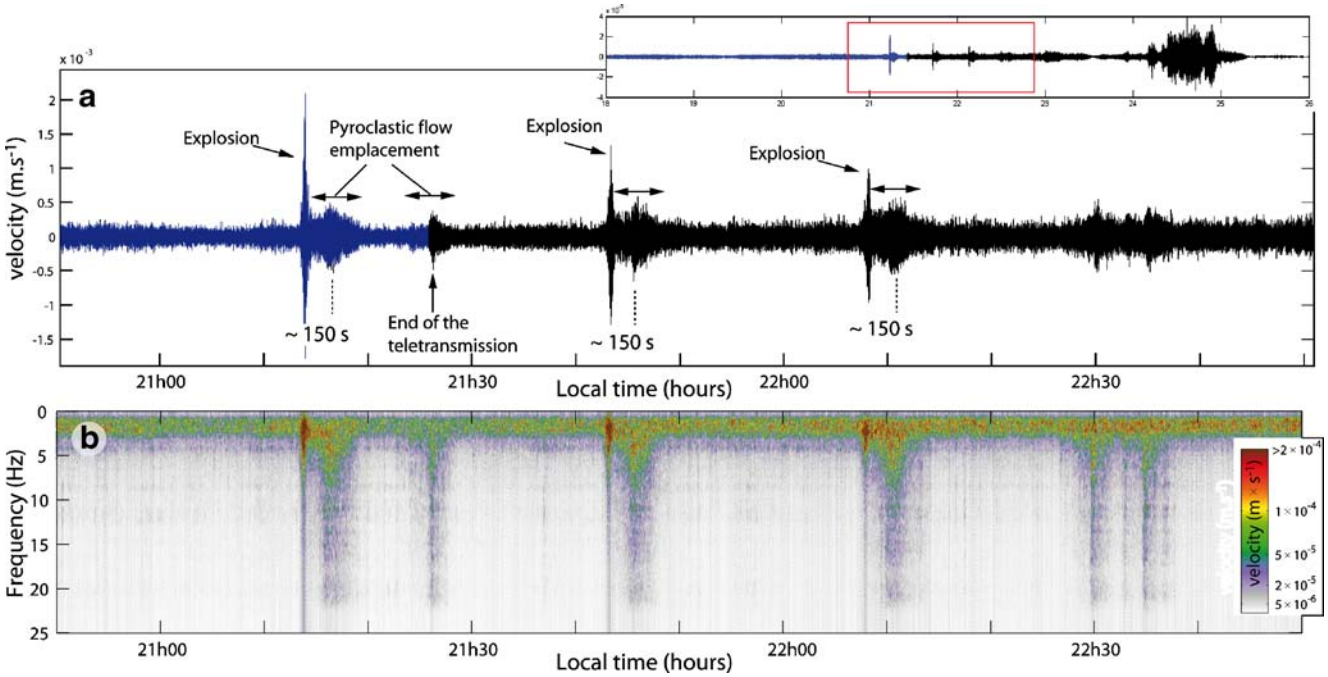

Fig. 4 Amplitude (**a**) and frequency (**b**) of seismic signals (*z*-component) recorded by the Cusua station (~4,500 m NW of the crater) between 2100 and 2300 hours. Initial pyroclastic flows were generated sporadically, either by explosions or not. The station was damaged by a pyroclastic flow at 2126 hours (*dark blue* signal transmitted to the observatory, *black* local record, transmission being cut by PF). Time delay between explosion and flow arrival is about 150 s, giving a pyroclastic flow velocity of about 30 m s^{-1}

We thus conclude that the signals described above are due to pyroclastic flows passing close by the seismic stations. As almost no signal has been recorded at Runtun, 600 m from the flow path, we hypothesise that the pyroclastic flows were only clearly detected where they passed by less than 200 m from the stations.

The same types of signals were recorded during the paroxysmal phase, with higher amplitude (Fig. 5). Seismic records thus confirm the visual observation that pyroclastic flows were generated continuously (but with pulses) over 40 min of the paroxysmal phase.

Velocity of pyroclastic flows and emplacement

IG-EPN scientists-in-charge at the observatory during the July 14th eruptions (P. Ramón and D. Barba) described the first pyroclastic flows as having a "low" velocity. Videos of July 14 and 15th pyroclastic flows allow us to estimate a velocity in the range of 20–30 m s^{-1}. Eyewitnesses of Achupashal flows on August 16th also spoke about "slow" flows but it is impossible to quantify flow velocity from these observations. Unfortunately, no clear video record exists for the August 16th pyroclastic flows since the paroxysmal phase occurred at night, and the volcano was almost completely covered by clouds.

However, seismic records allow us to estimate the velocity of the pyroclastic flows. At Cusua seismic station (~4.5 km from the crater), about 150 s separate the explosions from the maximal amplitude of the seismic signal generated by pyroclastic flows. This gives a mean velocity of about 30 m s^{-1}. This value is typical for this kind of pyroclastic flow (25–40 m s^{-1}, e.g. Hobblit (1986) at Mt St. Helens, USA; Yamamoto et al. (1993) at Unzen, Japan; Cole et al. (1998) at Soufrière Hills, Montserrat; Kelfoun et al. (2000) at Merapi, Indonesia). Geological observations also indicate that dense flows were generally constrained to the valleys and show limited runup around the curves, compatible with such a "low" velocity.

Source conditions and feeding rate

During the paroxysmal eruptive phase, continuous lava fountained up to 1,000 m high, and together with lava spilling out of the crater, it fed a continual stream of fragmented lava onto the cone's upper steep flanks. We believe that pyroclastic flows were formed by the gravitational mobilisation of all the bombs, scoriae and ash poured out around the crater by the fountain activity. The presence of a large apron of hot pyroclastic material after the eruption (Fig. 2) is compatible with this hypothesis. Where observations were possible, no explosion or fountain collapse was found to be the origin of the pyroclastic flows of the paroxysmal phase. Whatever the exact mechanism for the origin of the pyroclastic flow formation, visual observation indicates that they were formed under conditions of zero, or small, initial velocities.

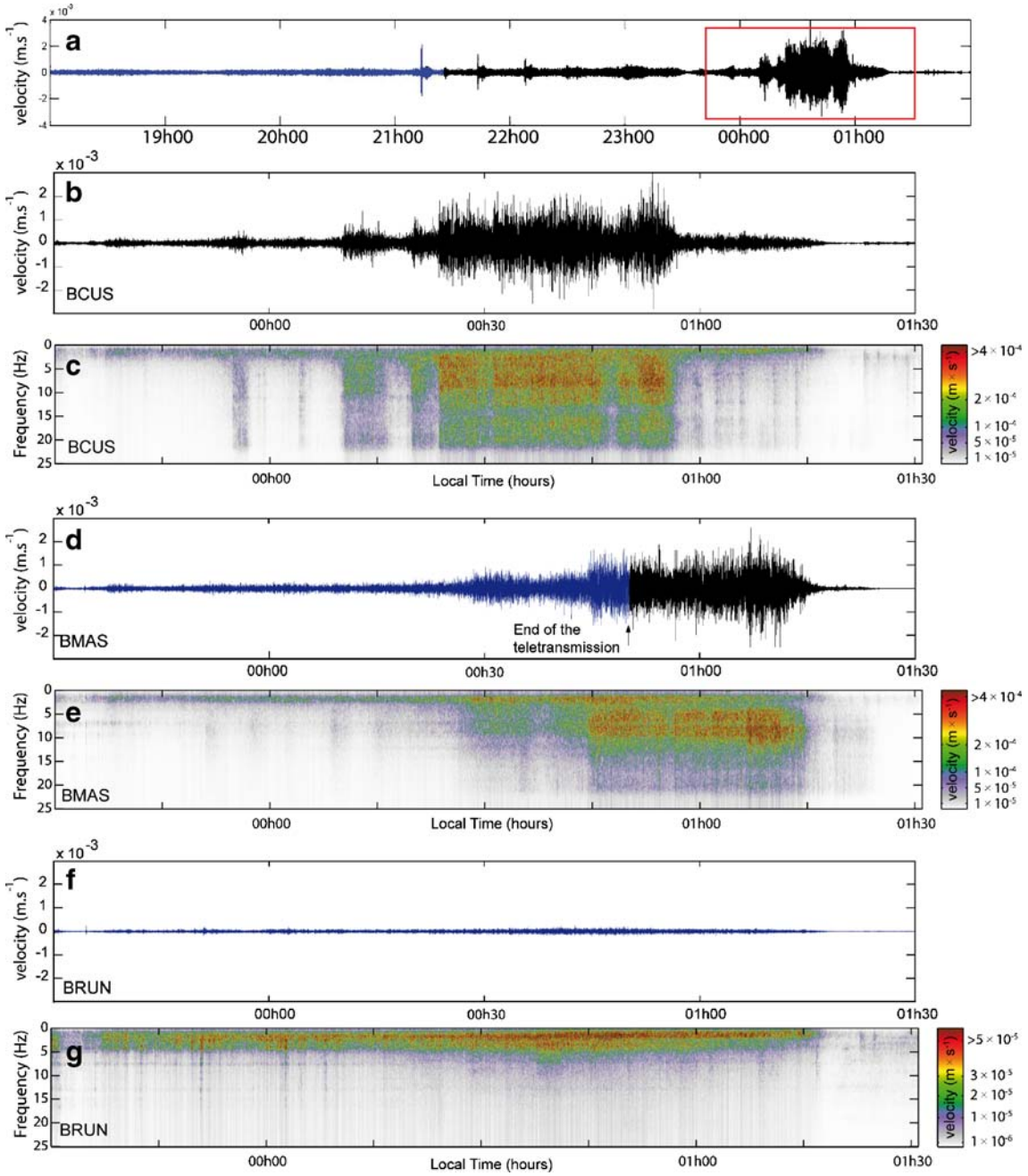

Fig. 5 Seismic records of three stations (*z*-component—Cusua, Mason and Runtun, Fig. 1) between 2330 and 0130 hours (local time), during the paroxysmal phase of the August 2006 eruption. Runtun, 600 m from the pyroclastic flow path, recorded a small amplitude signal. High-amplitude signals recorded by Cusua and Mason are not correlated: They are interpreted as being generated by different pulses of pyroclastic flows. *Dark blue* signal transmitted to the observatory, *black* local record, transmission being cut by pyroclastic flows

The main volume of pyroclastic flows was formed during a continuous phase that lasted about 40 min. The total volume of dense flows being $5–10\times10^6 m^3$, we assume the same volume for the paroxysmal phase given the small volume ($<10^6 m^3$) of sporadic pyroclastic flows previously emplaced. This gives a mean eruption rate of ~2,000–4,000 $m^3\ s^{-1}$.

The Cusua seismic station (~4.5 km, NW of the crater; Fig. 1) first recorded the pyroclastic flows of the continuous paroxysmal phase about 15 min before the nearer Mason station (3.5 km, S–W of the crater). This is related to the shape of the crater, which is lower to the northwest (~4,800 m asl) and indicates that pyroclastic flows were generated at increasing altitude during the first 15 min of

the paroxysmal phase, when the number of rivers affected increased. Flows were able to form on the north and south rim (~4,900 m asl) at about 0030 hours. At about 0055 hours, the eruption waned, pyroclastic flows shortened and were not able to reach the station of Cusua (4.5 km). However, between 0055 and 0120 hours, the station recorded flows that probably stopped some hundreds of metres from it (low amplitude of the signal, but still clearly detectable). Proximal pyroclastic flows continued to be detected with high amplitude at Mason, closer to the crater (3.5 km), 20 min (up to 0115 hours) after Cusua. Distant flows were detected at Mason and Cusua for a further few minutes, then the eruption stopped abruptly (end of pyroclastic flow, lava fountain and tremors). No pyroclastic flow was able to form on the eastern side of the cone, showing that the eruption was unable to form pyroclastic flows at heights greater than the east rim elevation (5,000 m asl).

It is hard to know exactly how the magma rate evolved over 40 min of paroxysmal activity. One hypothesis is that the magma rate increased with time, leading to an increase in the column height that generated pyroclastic flows. Another hypothesis is that the rate was approximately constant over the eruption period, but that a critical quantity of material needed to accumulate around the crater to trigger initiation of the pyroclastic flows. The lower points, covered by a larger quantity of fragmented lava, would have reached this critical threshold more rapidly. Pyroclastic flows shortened towards the end of the eruption, probably due to a decrease in magma rate.

Simulation of pyroclastic flows

Numerical model

Simulations are done with the code *VolcFlow* developed at the *Laboratoire Magmas et Volcans*. It is based on the depth-average approximation. Using a topography-linked coordinate system, with x and y parallel to the local ground surface and h vertical, the general depth-averaged equations of mass (Eq. 1) and momentum (Eqs. 2 and 3) conservation are:

$$\frac{\partial h}{dt}+\frac{\partial}{\partial x}(hu)+\frac{\partial}{\partial y}(hv)=0 \tag{1}$$

$$\frac{\partial}{\partial t}(hu)+\frac{\partial}{\partial x}(hu^2)+\frac{\partial}{\partial y}(huv) = gh\,\sin\alpha_x-\frac{1}{2}k_{\text{actpass}}\frac{\partial}{\partial x}\left(gh^2\cos\alpha\right)+\frac{T_x}{\rho} \tag{2}$$

$$\frac{\partial}{\partial t}(hv)+\frac{\partial}{\partial x}(hvu)+\frac{\partial}{\partial y}\left(hv^2\right) = gh\,\sin\alpha_y-\frac{1}{2}k_{\text{actpass}}\frac{\partial}{\partial y}\left(gh^2\cos\alpha\right)+\frac{T_y}{\rho} \tag{3}$$

where h is flow thickness, $\mathbf{u}=(u, v)$ is flow velocity, α is ground slope, $\mathbf{T}$ takes into account all the retarding stresses that slow down the flow (e.g. viscous, frictional and turbulent stresses), ρ is the bulk density of the pyroclastic flow (assumed to be 1,500 kg m^{-3}) and g is gravity (9.78 m s^{-2}). Subscripts denote components in the x and y directions (Table 1).

The parameter k_{actpass} is the earth pressure coefficient, the ratio of ground-parallel to ground-normal stress (see Savage and Hutter 1991). Its value is a function of the basal (between the avalanche and the ground surface) and the internal friction angle, φ_{bed} and φ_{int}, respectively, and is defined by Iverson and Denlinger (2001) by:

$$k_{\text{actpass}}=2\frac{1\pm\left[1-\cos^2\varphi_{\text{int}}(1+\tan^2\varphi_{\text{bed}})\right]^{1/2}}{\cos^2\varphi_{\text{int}}}-1 \tag{4}$$

This expression is only valid if $\varphi_{\text{bed}}\leq\varphi_{\text{int}}$. The sign ± is negative (and k_{actpass} active) where the flow is locally divergent and is positive (and k_{actpass} passive) where the flow is locally convergent. An isotropic stress is defined by $\varphi_{\text{int}}=0$ and $k_{\text{actpass}}=1$.

The terms on the right-hand side of the equations for momentum conservation indicate, from left to right, the stresses due to the weight, the pressure gradient and the retarding stress which depends on the rheological model chosen. The model allows for simulations of various rheologies, including frictional (with one or two friction angles), Bingham, viscous and Voellmy. More complex rheological laws can also be defined by the user.

For a dry frictional material, the retarding stress $\mathbf{T}$ is of the form:

$$T_x=-\rho h\left(g\cos\alpha+\frac{\mathbf{u}^2}{r}\right)\tan\varphi_{\text{bed}}\frac{u}{\|\mathbf{u}\|} \tag{5}$$

The term $\frac{\mathbf{u}^2}{r}$ takes into account the "overweight" due to the centrifugal acceleration on the topographic curvature (Savage and Hutter 1991). The term $-\frac{u}{\|\mathbf{u}\|}$ allows the x-component of the retarding stress in the direction opposed to the displacement to be calculated.

The equations were solved using a shock-capturing numerical method based on an upwind Eulerian scheme (Kelfoun and Druitt 2005). The scheme can handle shocks, rarefaction waves and granular jumps and is stable even on complex topography. Details and tests of the scheme are presented in more detail in Kelfoun and Druitt (2005). Additional details on the code, other results and downloadable files are shown on http://wwwobs.univ-bpclermont.fr/lmv/pperm/kelfoun_k/VolcFlow/VolcFlow.html

Table 1 Main variables used

Symbol	Variable	Value	Unit
g	Gravity	9.78	m s^{-2}
h	Flow thickness	–[a]	m
$k_{actpass}$	Earth pressure coefficient	–[a]	Dimensionless
S_i	Surface of the mesh I	–[a]	m^2
t	Time	–[a]	s
t_{erupt}	Duration of the flow genesis	2,400	s
V	Volume of pyroclastic flows	5×10^6–10^7	m^3
x, y	Space variables	–[a]	m
z_{gen}	Max elevation of flow genesis	5,000	m
$z_{rim,i}$	Elevation of the crater rim Upstream of the mesh i	–[a]	m
$\mathbf{T}=(T_x, T_y)$	Retarding stress of the flow	–[a]	Pa
$\mathbf{u}=(u, v)$	Flow velocity	–[a]	m s^{-1}
$\boldsymbol{\alpha}=(\alpha_x, \alpha_y)$	Ground slope	–[a]	degrees
φ_{bed}	Basal friction angle	0, 15 or 18	degrees
φ_{int}	Internal friction angle	0 or 30	degrees
ρ	Flow density	1,500	kg m^{-3}

[a] Varies during the calculation, in time or in space

Boundary conditions

Topography

The digital elevation model (DEM) was calculated by M. Souris (IRD) digitising then interpolating topographic maps (scale 1/50,000, elevation spacing 40 m) from the Military Geographic Institute of Ecuador. The DEM has a resolution of 10 m. Small topographic drainage features were smoothed locally by the interpolation process, and we have corrected them from field topographic measurements, for example, in the Mapayacu River drainage.

Source conditions

Several source conditions were investigated (increase of the rate with time, constant rate, final decrease etc.), fixing a feeding duration of 40 min (2,400 s) and a total volume of between 5×10^6 and $10^7 m^3$ according to field observations. We assumed that the pyroclastic flows formed close to the crater, and we fixed their source as being at the cells located just outside the crater rim, at a distance of 350 m from its centre (location x=783,940, y=9,837,550). The maximal elevation at which pyroclastic flows are generated was assumed to be z_{gen}=5,000 m, because no pyroclastic flows overflowed the eastern rim, at 5,000 m asl.

The results presented here were obtained with a volume of $10^7 m^3$ and with the simplest scenario, where the rate is constant with time. Further on we discuss other cases. Field observations indicate that a greater volume of pyroclastic flows formed at the low points of the rim than at higher points. We assume that the mass rate at the feeding cells, expressed by the variation of the thickness dh with time t, is a linear function of the difference between the maximal elevation, z_{gen}=5,000 m, where pyroclastic flows were generated and $z_{rim,i}$, the elevation of the crater rim taken radially between the mesh i and the centre of the crater.

$$\begin{cases} \frac{dh_i}{dt} = a\frac{\left(z_{gen}-z_{rim,i}\right)}{S_i} & \text{if } t \le 2,400 \text{ s} \\ \frac{dh}{dt} = 0 & \text{if} t > 2,400 \text{ s} \end{cases} \quad (6)$$

where S_i is the surface of the ith mesh, taking account of the DEM resolution and the local slope. The constant parameter a is calculated from the number of feeding cells, their elevation and the total duration of the eruption t_{erupt} to fit the total volume chosen. Using the 10×10-m-mesh DEM, there are 269 cells encircling the crater. If a volume $V=10^7 m^3$ is chosen, a is defined by

$$a = \frac{V}{t_{erupt}\sum_{i=1}^{269} z_{gen} - z_{rim,i}} \approx 0.121 m^2 s^{-1} \quad (7)$$

The new mass dh is assumed to be poured without velocity, the velocity of the cells at the feeding point being calculated by the conservation of momentum: $u_a = (u_b h_b + 0 \times dh)/(h_b + dh)$, where u_a and u_b are respectively the velocity after and before the new mass is added from the fountain. The parameter h_b is the thickness of pyroclastic material before the new mass is added.

Results

Frictional behaviour

With a basal friction angle alone (internal isotropic stress), the frictional model that best reproduces the extension of the August 2006 eruptions of Tungurahua assumes that $\varphi_{bed}=15°$. At the onset of the eruption, the mass poured on the crater rim immediately begins to flow and rapidly covers all the SW, W and NW flanks with a very thin layer of <<1 mm (Fig. 6a). Not only the main drainage channels are affected but also the interfluves. The mass accelerates along the steep (>30°) slope of the upper part of the cone, reaching a velocity of more than 150 m s^{-1}. The mean velocity of the front, which starts at 0 at the crater rim, is about 80 m s^{-1}, when the pyroclastic flows reach the seismic stations (red points on Fig. 6). The thickness of the pyroclastic flows on the interfluves does not significantly increase with time, but it does increase in the valleys into which the mass drains (Fig. 6b, c). The mass begins to decelerate and accumulate where the slope is less than the friction angle. After the source stops, at t=2,400 s, all the mass deposited on the flank rapidly drains down and accumulates at the foot of the volcano on slopes slightly lower than the friction angle (Fig. 6c, f). There it forms "sand piles" with a surface angle of about 15° (Fig. 7).

Figure 8 illustrates the morphology in cross section of the deposits obtained with the frictional model. The topography of the zoomed area has been artificially smoothed to avoid small-scale perturbations, thus demonstrating the typical morphology of a flow with a frictional behaviour. A very thin wedge of material runs rapidly on slopes steeper than 15° (the basal friction angle chosen). Where the slope of the flow surface is less than 15° (x~370 m, not visible on the figure), the flow begins to slow down and rapidly stops. The mass then

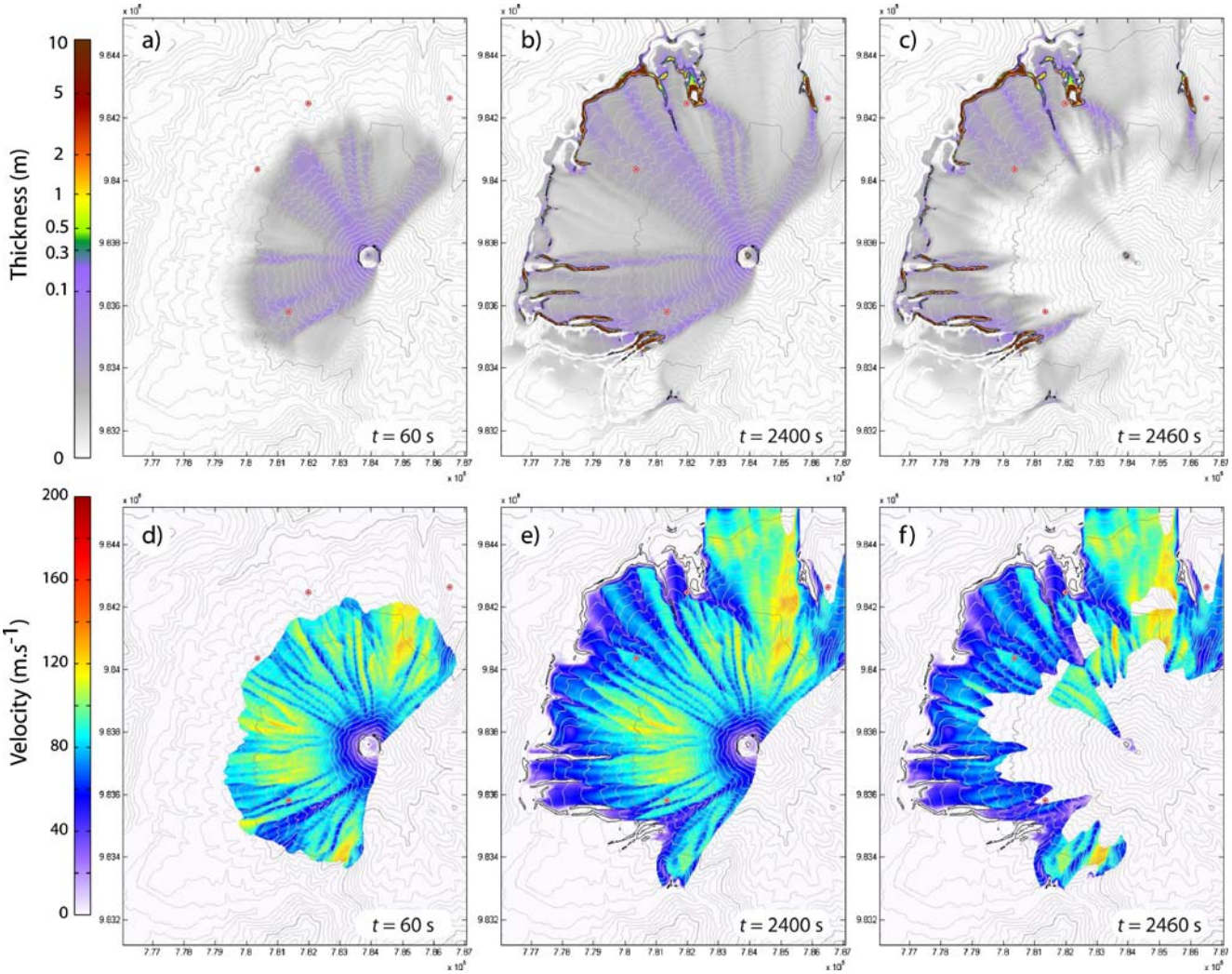

Fig. 6 Thickness (**a**–**c**) and velocity (**d**–**f**) of pyroclastic flows at Tungurahua simulated using the frictional model ($\phi_{bed}=15°$) at t=60 (**a**, **d**), 2,400 (**b**, **e**) and 2,460 s (**c**, **f**). The *colour scale* of the thickness (**a**–**c**) is logarithmic. *Black contours* indicate 0.1 m deposits (no thinner pyroclastic flow deposits were observed in the field). For clarity, velocity is only drawn where the mass is thicker than $1e^{-6}$m

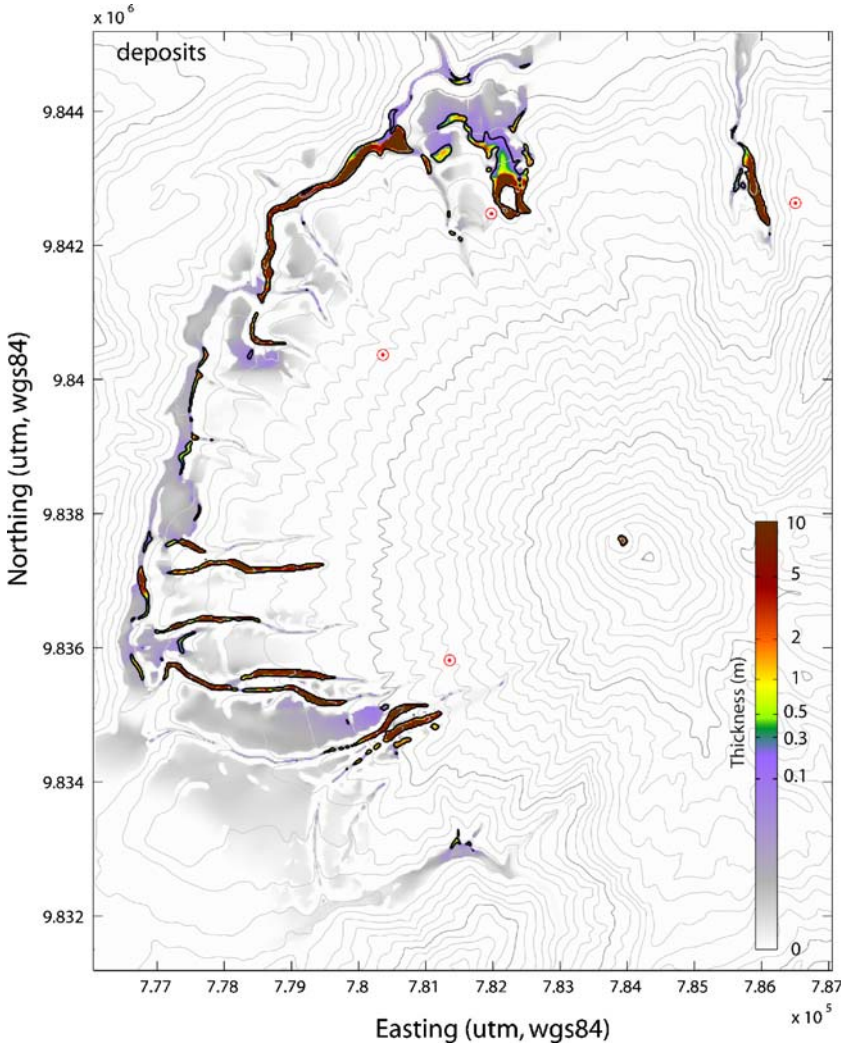

Fig. 7 Thickness of pyroclastic flow deposits of Tungurahua simulated using the frictional model (ϕ_{bed}=15°). The mass accumulates on slopes slightly lower than the friction angle (15°) to form sand pile-like deposits

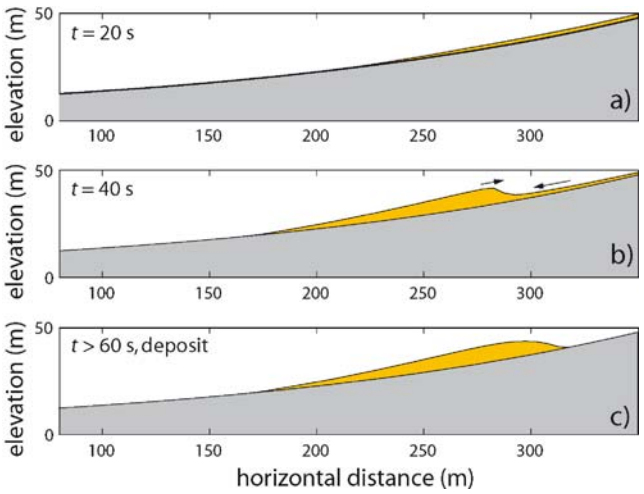

Fig. 8 Typical emplacement of flow and deposit using the frictional model. The mass accumulates on slopes slightly lower than the friction angle (15°) to form sand pile-like deposits. Time is counted from the instant the flow enters the frame (x=350)

accumulates upstream forming a pile with slopes of about 15° (less on the downstream side due to inertia). This behaviour explains the accumulation and the shape of simulated pyroclastic material at the downstream margin of the affected area.

The same behaviour arises using any combination of both internal and basal friction angle (Fig. 9a). The internal angle modifies the effect of the pressure gradient (changing the value of $k_{actpass}$, Eqs. 2, 3 and 4) and thus slightly decreases velocity and runout. However, this effect is small because the flows are very thin compared to the variations of the volcano topography and the stress of the pressure gradient if thus negligible compared to the stress of the weight. This is why results obtained with only one friction angle (φ_{bed}=15°, φ_{int}=0°) are very similar to results obtained with two friction angles (φ_{bed}=15°, ϕ_{int}=30°). A high value of the internal angle is also difficult to reconcile with the apparently high internal fluidity of natural pyroclastic flows.

Changing the velocity of the source does not change the behaviour described above. Figure 9b shows the results

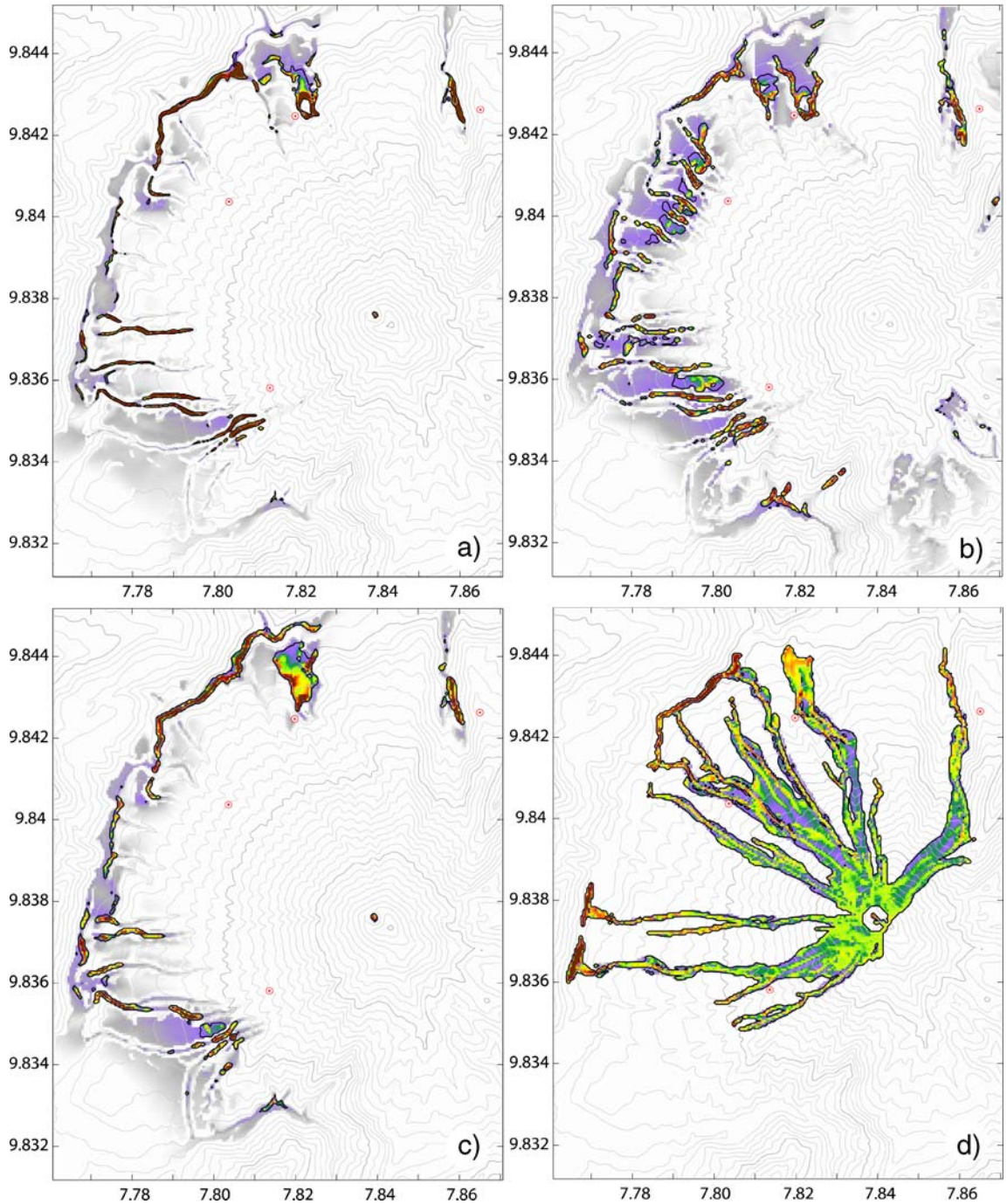

Fig. 9 **a** Simulation of pyroclastic flows with a two friction-angle frictional rheology (φ_{bed}=15° and φ_{int}=30°; same DEM resolution as Figs. 6, 7, 10 and 11). **b–d** Simulations on a lower-resolution topography (50 m). **b** Frictional rheology with one friction angle (φ_{bed}=18°) and a very high (and unrealistic) velocity of 100 m s^{-1} over 2,400 s at the source. **c** Frictional rheology with one friction angle (φ_{bed}=15°; conditions are similar as Fig. 7). **d** Constant retarding stress rheology (**T**=5 kPa; conditions are similar as Fig. 11)

obtained if a very high initial velocity is imposed on the flow (100 m s^{-1} at the source over 2,400 s, which is much higher than what could be inferred from observation). The basal friction angle must be increased (to 18°) to slow down the flow enough to reach the same runout as previously, but the flows still accumulate at the downstream margin to form deposit piles.

Constant retarding stress

As discussed below, the behaviour simulated using the frictional model is very different to that observed in the field. The same difference in behaviour was detected by Kelfoun and Druitt (2005) for their simulation of the Socompa debris avalanche: The frictional model was unable

to reproduce, even to the first order, the emplacement of the avalanche. It formed "dunes" or "hummock"-like piles on the gentler slopes. They showed that a constant retarding stress (Dade and Huppert 1998), also called yield strength, is very much more appropriate than frictional behaviour and enabled all the main features of the avalanche deposit to be reproduced. We have thus tried to simulate the pyroclastic flows at Tungurahua using this simple rheological law.

This empirical law simply states that the retarding stress is constant, independent of the velocity, the thickness or any other parameter of the flow:

$$T_x = \text{Constant} \times -\frac{u_x}{\|u\|} \text{ or } T = \left\|\vec{T}x + \vec{T}y\right\| = \text{Constant} \tag{8}$$

Figure 10 illustrates the emplacement of constant stress pyroclastic flows using the same source conditions as for Figs. 6 and 7. The best fit results are obtained with a constant retarding stress of 5 kPa.

The first difference with the frictional model is that the mass accumulates around the rim before reaching a critical thickness of about 0.5 m, at which point flow is initiated. Simulated flows present a thickness close to the thickness of natural pyroclastic flows (0.5–2 m thick) and are restricted to the valleys (Fig. 10a–c).

Figure 10d–f shows that emplacement of numerical flows is carried out by pulses (see arrows on Fig. 10e, clearest on additional movie material) even if the source rate is constant: The mass accumulates until it reaches a critical thickness (about 0.5 m) which allows flow to take place. The mass then reaccumulates until the critical thickness is reached and a new pulse forms. Numerical pulses are thicker and faster than the neighbouring material and generally run at less than 30 m s^{-1}.

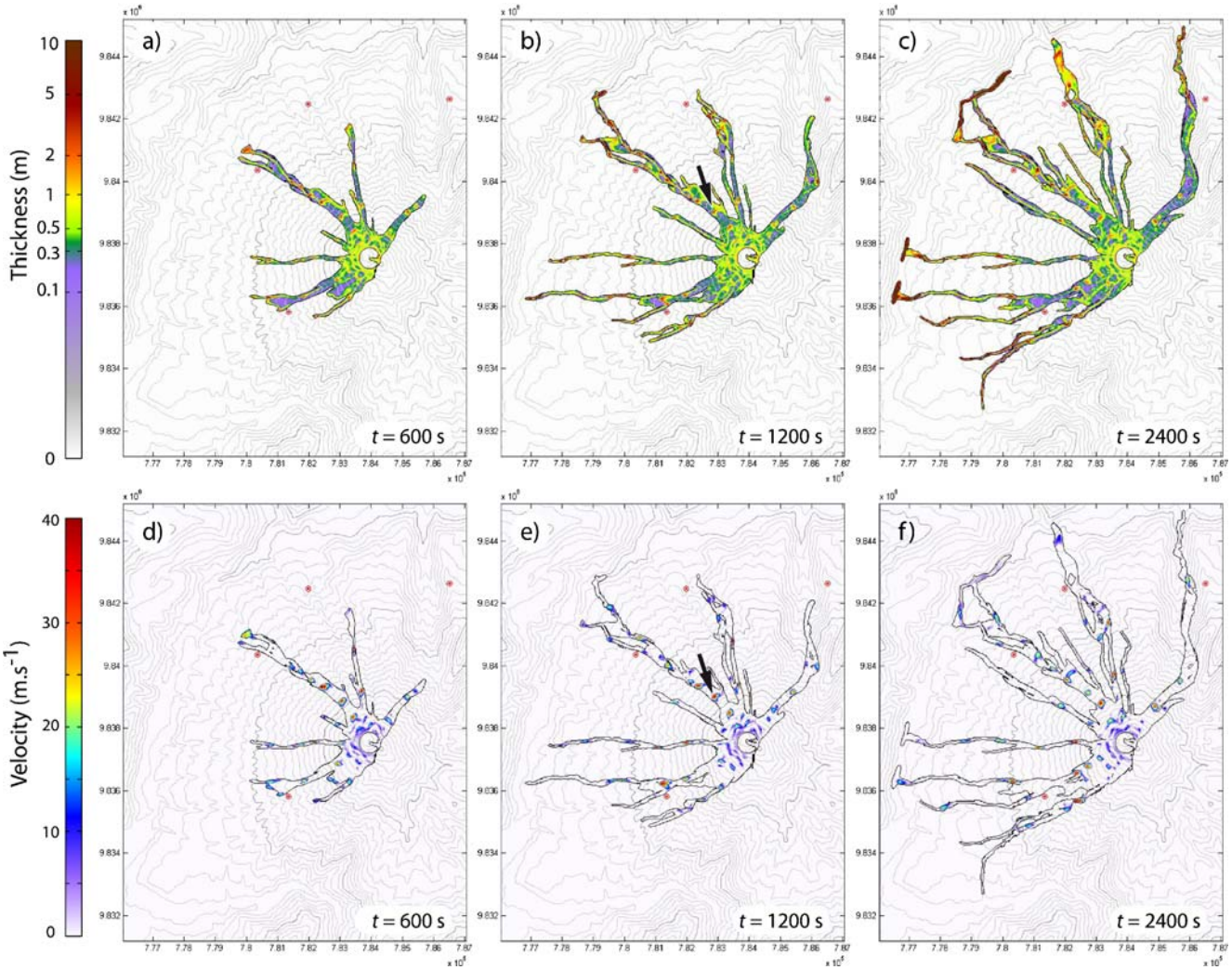

Fig. 10 Thickness (**a**–**c**) and velocity (**d**–**f**) of pyroclastic flows at Tungurahua simulated using the constant stress model (5 kPa) at t=600 (**a**, **d**), 1,200 (**b**, **e**) and 2,400 s (**c**, **f**). The *colour scale* of the thickness (**a**–**c**) is logarithmic. *Black contours* indicate 0.1 m deposits (no thinner pyroclastic flows were observed on the field). *Arrows* locate a pulse characteristic of the emplacement of constant-stress flows

The fronts of the flows are well defined during emplacement. The simulated deposits also show a well-defined front and a progressive decrease of the thickness on steeper slopes (Fig. 11). Figure 12 illustrates the typical form of a flow formed by a constant retarding stress using the same topography as Fig. 8.

Discussion

Frictional model

To a first approximation, the area of deposit generated by the frictional model covers that of natural pyroclastic flow deposits. However, a critical analysis of the results demonstrates that the frictional model is unable to reproduce accurately the behaviour of the dense pyroclastic flows of Tungurahua. The geometry of the deposits obtained from numerical modelling does not resemble that of the natural deposits. Simulated flows are present in the valleys as well as on the interfluves, whereas the latter one remained uncovered by the natural dense flows. We stress that the frictional model only simulates dense flows and that it is unable to reproduce ash-cloud or ash-cloud surge physics. The local resemblance between simulated deposits and natural ash deposits cannot be considered as a validation of the model. Simulated deposits appear as piles accumulated at the foot of the volcano or on gentle valley slopes, rather than as a continuously distributed layer with a small increase in thickness downstream. The very thin wedge of the simulated front (<<1 mm) is also quite unlike those observed in the field.

The simulated velocity of pyroclastic flows (more than 150 m s^{-1}) appears to be incompatible with field observations at Tungurahua, as well as for other volcanoes in the world for dense flows of this volume and thickness (e.g. Hobblit 1986; Yamamoto et al. 1993; Cole et al. 1998; Kelfoun et al. 2000). This is explained by the fact that a frictional body accelerates on slopes steeper than its frictional angle: a drop of about 2,000 m in the case of

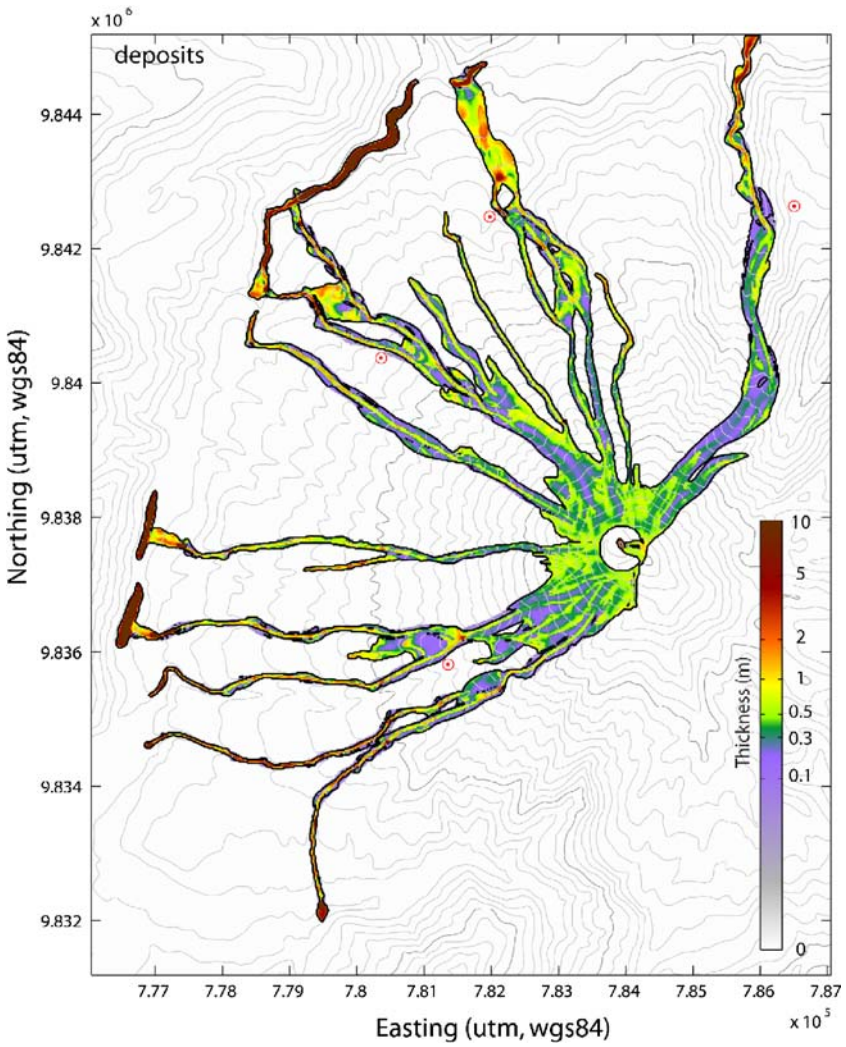

Fig. 11 Thickness of pyroclastic flow deposits at Tungurahua simulated using the constant retarding stress model (5 kPa). The thickness and geographic distribution of deposits resemble the field observations

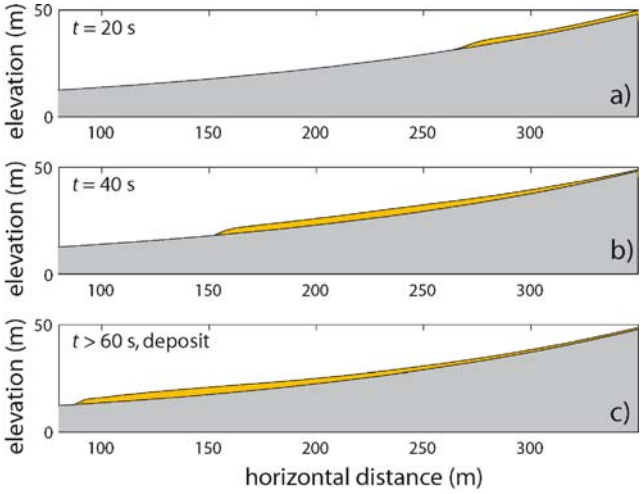

Fig. 12 Typical emplacement of flow and deposit with the constant-stress model. The front is well defined and the thickness progressively decreases upstream. Time is counted from the instant the flow enters the frame (x=350)

Tungurahua, with an acceleration over a distance of about 4,500 m horizontally. Quasiconstant velocity can be reached with a frictional behaviour (e.g. Pouliquen and Forterre 2002) but only with a slope close to the friction angle of the material and not on volcanoes whose slopes typically change from >30° near the crater to less than 5° where the pyroclastic flows stop. With such a high velocity, pyroclastic flows cannot be confined to the valleys and rapidly overflow the interfluves. It is physically meaningless to maintain a frictional regime at such a high velocity and with such a small thickness, but this is implicit in using a simple frictional rheology for pyroclastic flow simulation.

We should emphasise that the incompatibility between numerical results and field data is not due to a problem in the numerical code: Put a grain of frictional material (sand for example) on the surface of a curved slope covered by the same material and the grain will immediately slide down the slope and will stop just beyond where the slope becomes less than the friction angle of the material. Several grains together will all still stop at approximately the same place. Pour the sand over some tens of seconds and the sand will flow and accumulate to form a sand pile. Our frictional results reproduce exactly this frictional behaviour. The "sand pile" shape of flows and deposits can also be observed in the simulations of granular flows in the laboratory (e.g. Pudasaini and Hutter 2006, and reference therein) and in pyroclastic flows using frictional behaviour (e.g. Patra et al. 2005). This last study, however, mainly focuses on the numerical scheme and does not aim to prove whether or not the frictional model is suitable for pyroclastic flows. The numerical results which they obtained were not subsequently compared to the thickness, distribution and morphology of natural deposits.

It should also be noted that all the characteristics described here which show that frictional behaviour differs from natural pyroclastic flows are largely independent of the total volume, feeding conditions, topography and friction angle (see Fig. 9). The same behaviour occurs when the rate, the volume or the way the mass is injected are changed. This conclusion can also be demonstrated with sand in the laboratory: Pouring sand twice as much down a curved slope does not fundamentally change the fact that the flow will accelerate on a slope steeper than the friction angle or that deposits will not be present on these slopes and that the sand will accumulate downstream in a pile. The frictional model is largely independent of the thickness of the flow (the effect of the pressure gradient only) and this is why initial conditions (e.g. volume and rate variations) have little influence on the simulated flows. With a friction angle less than or greater than 15°, the same behaviour occurs, but the distances reached by simulated flows are respectively greater and smaller than in reality. Results of the frictional rheology are also poorly influenced by the resolution of the topography. Figure 9c was carried out with a low-resolution topography (50 m) and simulated deposits are very similar to those presented on Fig. 7. Small differences arise mainly downstream of the narrowest drainage channels, which could not be reproduced accurately enough with a low resolution.

If the source conditions are changed to simulate an increase of the level at which pyroclastic flows were generated with time, the results are slightly improved: The first simulated flows occurred on the NW flank and flows progressively affected the northern and the southwestern flanks, as was the case in reality. However, this does not change the conclusions about the shape of the flows and the deposits, nor the overly high velocity.

The entrainment of accidental clasts does not change our conclusions either. The entrainment would play an important role in the momentum balance of the flows (e.g. in Mapayacu valley) and could shorten the distance they will reach. The best-fit value (of the friction angle and of the constant retarding stress) must then be lowered to reach the natural runout, but the shape of deposits remain similar: Even with a low velocity, a 15° frictional flow is unable to deposit on slopes steeper than 15° (moreover, this value would be lowered due to the mass entrained, in order to compensate for the loss of momentum).

Finally, it should be noted that all the problems raised here are not dependant on conditions particular to Tungurahua, but rather on slope variations which are common to most volcanoes: a slope decreasing from about 30° to few degrees over a distance of several kilometres. Therefore, we think that the discrepancies between the deposits simulated with the frictional model and natural deposits of pyroclastic flows apply to more than just the individual case of Tungurahua.

An important point to underline is that our results do not contradict the results obtained by previous authors who reproduced granular flows with the frictional model (e.g. Iverson et al. 2004; Denlinger and Iverson 2004; Pudasaini and Hutter 2006, and references therein). The good fit they obtained is based on flume or laboratory experiments with sand, eventually adding water. In this case, they have demonstrated that the frictional behaviour plays an important role in the dynamics. What our results show is that the behaviour of natural pyroclastic flows differs from the behaviour of granular flows at a smaller scale. This may be due to the high temperature, the high polydispersity, the presence of very fine particles, the duration of the emplacement or the high volumes involved.

Our results thus underline the problem of using the frictional model for hazard assessment. One could argue that the actual shape of deposits is not important for hazard assessment and that a good map of "inundation" can be obtained with a simple model that does not reproduce the morphology of the phenomenon. However, our results show that the frictional model cannot create a correct inundation map, either. With the frictional model, all the interfluves are affected by numerical dense flows whereas in natural flows, dense flows are restricted to valleys (interfluves may be affected by surges but the frictional model is not able to simulate them). The simulated mass also accumulates in thick piles (up to 50 m) and cannot spread. The model thus underestimates the hazard over a flat area. Finally, the frictional model achieves velocities five times higher than in reality. It is these unrealistically high velocities which enabled simulated flows to cross ridges that they would not be able to cross in reality. The portion of the flow which crosses the ridge is no longer available to follow the drainage and to affect downstream areas. Thus, where valleys deviate from a straight plan view, the frictional model can greatly underestimate downstream areas affected. This occurred on the south flank of Tungurahua, where the simulated flows accelerated on the steep slopes of the terminal cone. The unrealistically high velocity allowed the flows to escape from the Mapayacu River valley and cross the 100-m-high barriers that bound it. The flows then formed deposits to the south (purple to red deposits to the south in Fig. 7); in reality, these areas are unaffected. The mass lost due to this overly high velocity was no longer present in the Mapayacu River. Hazards are thus underestimated at the mouth of the river and in the neighbouring area of the Palitahua village (Fig. 1).

Constant retarding stress model

Our results indicate that a constant stress rheology reproduces to first order the main characteristics of observed pyroclastic flows. The deposits simulated with this rheology are restricted to valleys, and affected areas in the model are similar to those areas affected in reality. The shapes of flow fronts and deposits are closer to reality than for the frictional model and velocity of the pulses is about 30 m s^{-1}, as has been observed.

Some other characteristics of our constant retarding stress simulations appear compatible with field observation. The simulated flow is composed of pulses, each flow having a velocity close to observed velocities. The pulse emplacement of simulated flows appears compatible with pulses observed during emplacement and with lobes and units observed in the field deposits (Fig. 3c). However, we cannot confirm that the frequency of generation or the distance run by each pulse is realistic. The velocity of the simulated front is slow, the flows passing close to the seismic stations about 500 s after the formation of the column, giving a mean velocity of the front of the flows of less than 10 m s^{-1} (the flows being composed of successive pulses with a velocity of 30–40 m s^{-1}). This differs from the 150 s measured for the flows formed by explosions. However, we lack data about the time delay between the initiation of the fountain and the first arrival of pyroclastic flows at the seismic stations, our quantification only concerning explosive events. If, in reality, the mass had to accumulate before flowing, our simulation appears correct. Note that a time of about 150 s can be obtained with the model if a mass of more than $5\times10^4 m^3$ is poured out immediately upstream of a valley, showing that the constant retarding stress model is compatible with the velocity of explosion-generated pyroclastic flows.

The main difficulty in using the constant retarding stress model is its strong dependence on source conditions (volume, rate) and on the topography. This is mainly because the flow capacity of the model is directly related to the thickness of the flows, a thicker flow being very mobile, a thin flow being able to stop on slopes (the flow capacity depends on the difference between the driving force which increases with thickness and the retarding stress that remains constant). If the resolution of the DEM is too low, the shape of the valley is not estimated correctly. In our model, the valleys in the DEM are larger and smoother than in reality. Deposits spread much further laterally, some reaching up to 50 m in width in the model, whereas they are less than 10 m wide in the field. Because the surface of deposition is wider than in reality, not enough mass is available to reach the natural runout if we use the value of the constant retarding stress that would have been obtained on a perfect topography. To reach the natural runout, the value of the constant retarding stress must be reduced, thus reducing the simulated thickness of deposit. This is why, using the volume estimated for the whole deposit, the simulated thickness approximately corresponds to the thickness of one unit (0.5–2 m) but not to the total thickness of

deposits (~5–10 m). This value of 5 kPa is, however, interesting because it gives an estimation of the rheological behaviour of each pyroclastic flow pulse at Tungurahua.

The sensitivity of the constant retarding stress to the resolution of the topography is illustrated in Fig. 9d, where the resolution of the DEM has been reduced at 50 m. It is particularly clear in the southern drainage channels where the valleys are narrow: The poor resolution chosen for Fig. 9 (50 m) forms wider and smoother valleys. The simulated flows spread out too much and start laying down deposits on higher slopes, leaving too little mass available to achieve the runout of the natural flows. With this resolution, the runout distance could only be reached by lowering the value of the constant retarding stress (thus thinning deposits). The low quality of the topography upstream of the small rivers (Bilbao/Chontapamba for example) also explains why the pyroclastic flows in these areas have not been simulated accurately.

The quality of the simulations is clearly dependant on the accuracy and the resolution of the digital topography used. However, whatever the quality of the topography, the characteristics of the constant retarding stress simulations (thickness variations, velocity, shape of the front, geographic distribution of deposits) are much closer to natural phenomena than simulations carried out with the frictional behaviour (Fig. 9).

A similar conclusion has been drawn by Kelfoun and Druitt (2005) for the simulation of the avalanche of Socompa: The main features of the Socompa avalanche (morphology, thickness and lithology distribution) can be reproduced successfully by a constant retarding stress rheology, whilst they are impossible to reproduce with the frictional rheology. The value obtained for the pyroclastic flows of Tungurahua, 5 kPa, is, however, ten times smaller than the value of about 50 kPa of Kelfoun and Druitt (2005). At present, we cannot physically explain this difference. It does seem though that the value of the constant retarding stress is directly related to the thickness of deposits. The higher the value of the constant retarding stress, the thicker the deposits formed. Debris avalanche deposits that are thicker than pyroclastic flow units should thus be simulated with a higher value of the constant retarding stress.

Other rheological laws

Other rheological laws have been used to simulate pyroclastic flows or other geophysical flows. Here, we briefly describe how appropriate they are for Tungurahua pyroclastic flows.

Some authors have used more complex frictional laws. Pouliquen and Forterre (2002) have shown that, even in the laboratory, the rheology of sand is more complex than simple friction. Their results show that the friction angle depends on the velocity and the thickness of the flow. Heinrich et al. (2001) used a partial form of the law of Pouliquen and Forterre (2002) to simulate a debris avalanche at Montserrat. At Tungurahua, the partial form of the law fails to reproduce the deposits mainly because it neglects the strong increase in the friction angle when the speed of the flow decreases: Where the flow slows down, the friction angle decreases and all the mass drains onto the lowest slopes and accumulates in piles. Flow velocities and deposits are, however, closer to natural phenomenon than with the simple friction law. The complete form of the law appears to be better suited, but we were unable to find a combination of the six free parameters that fitted the natural deposits more closely than we reproduced with the constant stress condition. Note that the complete form of the law could produce a behaviour close to the constant retarding stress as the friction coefficient φ decreases when the thickness h increases. It could then be possible for the frictional retarding stress to remain approximately constant whilst the friction angle varies (see "Introduction" section).

A viscous material allows a velocity compatible with field observations to be reached and flows are constrained to the valleys. However, such material cannot form deposits, as all the mass escapes from the investigated area since a viscous flow cannot stop on slopes.

The law combining frictional behaviour with a velocity-dependent retarding stress (e.g. McEwen and Malin 1989; Wadge et al. 1998) allows the velocity of the flows to be limited and appears to be better adapted than a simple frictional law. However, to reach the runout distance, the friction angle has to be lower than 15°. The mass then drains down steeper slopes and forms pile deposits at the foot of the volcano. The Voellmy law, also combining a frictional stress with a velocity squared dependent stress (e.g. Evans et al. 2001), gives the same kind of behaviour and deposits.

Bingham flow, a constant retarding stress plus a viscous stress, gives a good fit with reality if the viscosity is low (<1,000 Pa s). The lack of accuracy of source and topographic conditions does not allow us to state whether this model, proposed by other authors for pyroclastic flows (e.g. Sparks 1976; Freundt and Schmincke 1985), is better or not, or to give a value of the most appropriate viscosity. For the same reason, we cannot exclude that results would be better if a small turbulent stress or collisional stress were added to the constant retarding stress.

We stress that only simple rheological laws have been studied. More complex laws involving, for example, degassing or sedimentation can present behaviour that appears to approximate flow behaviour and natural deposits. Different laws exist which each contain several free parameters, and we were not able to find a combination of parameters that fitted the observations better than with the constant retarding stress condition. These laws are, more-

over, outside the scope of this paper, which aims instead to analyse simple rheological models that can be used for hazard assessment.

Conclusions

A comparison between simulations and well-constrained field data shows that the frictional model cannot simulate pyroclastic flow emplacement and deposits at Tungurahua volcano. We also believe that this conclusion is not restricted to this field case alone because the inadequacy is mainly related to a slope variation which is common to many volcanoes. Friction between the particles that compose pyroclastic flows probably exhibits a Mohr–Coulomb behaviour but it seems that other phenomena act on the dynamics to give a much more complex behaviour to the flow.

The constant retarding model appears to simulate pyroclastic flows much better than the frictional model. The main weak point of the constant stress model is that it is empirical and does not have a physical basis. It should thus be used carefully. We think, however, that the greater suitability of the constant retarding stress proves that the ratio of driving/retarding stress cannot be considered as constant—as for the frictional model—but decreases as the thickness increases. Above a certain thickness, the flow is able to move. Below this thickness, the retarding stress dominates the driving stress and the flow slows down. This produces flow deposits with a more or less constant thickness as seen in the field.

The physics of pyroclastic flows is complex and further research is needed to understand it fully and to obtain a robust physical model. Our results are useful in that they should place constraints on any future, more complex model which would need to explain why a constant stress model is much better adapted than a frictional model for simulating pyroclastic flows. In the meantime, the frictional model appears to be too simple to be used for pyroclastic flow simulations and we believe that it cannot be used for hazard assessment. Constant retarding stress possibly represents an acceptable alternative.

Acknowledgements Those studies have been funded by the French *Institut de Recherche pour le Développement* (IRD). We thanks the *Japan International Cooperation Agency* (JICA) and Dr Hiroyuki Kumagai for the use of seismic data. The paper was improved by Fran van Wyk de Vries and by the useful comments of A. Neri, M. Bursik, an anonymous reviewer and the editor. The authors deeply thank the staff of the Tungurahua Volcano Observatory (IG-EPN), especially those in charge during the July 14th and August 16th eruptions.

References

Burgisser A, Bergantz GW (2002) Reconciling pyroclastic flow and surge: the multiphase physics of density currents. Earth Planet Sci Let 202:405–418

Cole PD, Calder ES, Druitt TH, Hoblitt R, Robertson R, Sparks RSJ, Young SR (1998) Pyroclastic flows generated by gravitational instability of the 1996–97 lava dome of Soufriere Hills Volcano, Montserrat. Geophys Res Let 25(18):3425–3428

Dade WB, Huppert HE (1998) Long-runout rockfalls. Geology 26:803–806

Dartevelle S (2004) Numerical modeling of geophysical granular flows: 1. A comprehensive approach to granular rheologies and geophysical multiphase flows. Geochem Geophys Geosys 5(8): Q08003. doi:10,1029/2003GC000636

Denlinger RP, Iverson RM (2004) Granular avalanches across irregular three-dimensional terrain: 1. Theory and computation. J Geophys Res 109:F01014. doi:10.1029/2003JF000085

Evans SG, Hungr O, Clague JJ (2001) Dynamics of the 1984 rock avalanche and associated distal debris flow on Mount Cayley, British Columbia, Canada; implications for landslide hazard assessment on dissected volcanoes. Eng Geol 61:29–51

Freundt A, Schmincke HU (1985) Lithic-enriched segregation bodies in pyroclastic flow deposits of Laacher See volcano (East Eifel, Germany). J Volcanol Geotherm Res 25:193–224

Gray JMNT, Tai YC, Noelle S (2003) Shock waves, dead zones and particle-free regions in rapid granular free-surface flows. J Fluid Mech 91:161–181

Hall ML, Robin C, Beate B, Mothes P, Monzier M (1999) Tungurahua Volcano, Ecuador: structure, eruptive history and hazards. J Volcanol Geothermal Res 91(1):1–21

Hall ML, Mothes PA, Ramon P, Arellano S, Barba D, Palacios P (2007) Dense pyroclastic flows of the 16–17 August 2006 Eruption of Tungurahua Volcano, Ecuador. AGU Joint Assembly, Acapulco, Mexico

Heim A (1882) Der Bergsturz von Elm. Z Dtsch Geol Ges 34:74–115 (in German)

Heinrich P, Boudon G, Komorowski JC, Sparks RSJ, Herd R, Voight B (2001) Numerical simulation of the December 1997 debris avalanche in Montserrat, Lesser Antilles. Geophys Res Lett 28:2529–2532

Hobblit RP (1986) Observations of the eruptions of July 22 and August 7, 1980, at Mount St. Helens, Washington. USGS Prof Paper, 1335

Hsü J (1975) Catastrophic debris streams (sturzstroms) generated by rockfalls. Geol Soc Amer Bull 86:129–140

Iverson RM, Denlinger RP (2001) Flow of variably fluidized granular masses across three-dimensional terrain 1. Coulomb mixture theory. J Geophys Res 106:537–552

Iverson RM, Logan M, Denlinger RP (2004) Granular avalanches across irregular three-dimensional terrain: 2. Experimental tests. J Geophys Res 109:F01015. doi:10.1029/2003JF000084

Kelfoun K, Druitt TH (2005) Numerical modeling of the emplacement of Socompa rock avalanche. Chile. J Geophys Res 110:B12202. doi:10.1029/2005JB 003758

Kelfoun K, Legros F, Gourgaud A (2000) Statistical study of damaged trees related to the pyroclastic flows of November 22, 1994 at Merapi volcano (central Java, Indonesia): relation between ash-cloud surge and block-and-ash flow. J Volcanol Geothermal Res 100:379–393

Kumagai H, Yepes H, Vaca M, Caceres V, Nagai T, Yokoe K, Imai T, Miyakawa K, Yamashina T, Arrais S, Vasconez F, Pinajota E, Cisneros C, Ramos C, Paredes M, Gomezjurado L, Garcia-Aristizabal A, Molina I, Ramon P, Segovia M, Palacios P, Troncoso L, Alvarado A, Aguilar J, Pozo J, Enriquez W, Mothes P, Hall M, Inoue I, Nakano M, Inoue H (2007) Enhancing volcano-monitoring capabilities in Ecuador. Eos Trans AGU 88 (23):245

Le Pennec JL, Jaya D, Samaniego P, Ramón P, Moreno Yánez S, Egred J, van der Plicht J (2008) The AD 1300–1700 eruptive periods at Tungurahua volcano, Ecuador, revealed by historical

narratives, stratigraphy and radiocarbon dating. J Volcanol Geotherm Res 176:70–81

McEwen AS, Malin MC (1989) Dynamics of Mount St. Helens' 1980 pyroclastic flows, rockslide-avalanche, lahars, and blast. J Volcanol Geotherm Res 37:205–231

Mothes PA and staff IG-EPN (2007) Tungurahua Volcano's 1999–2007 eruptive process, monitoring results and risk mitigation. AGU, Joint Assembly, Acapulco, Mexico

Neri A, Ongaro TO, Macedonio G, Gidaspow D (2003) Multiphase simulation of collapsing volcanic columns and pyroclastic flow. J Geophys Res 108(B4):2202. doi:10.1029/2001JB000508

Patra AK, Bauer AC, Nichita CC, Pitman EB, Sheridan MF, Bursik M, Rupp B, Webber A, Stinton AJ, Namikawa LM, Renschler CS (2005) Parallel adaptive numerical simulation of dry avalanches over natural terrain. J Volcanol Geotherm Res 139(1):1–22

Patra AK, Nichita CC, Bauer AC, Pitman EB, Bursik M, Sheridan MF (2006) Parallel adaptive discontinuous Galerkin approximation of the debris flow equations. Comput Geos 32:912–926

Pouliquen O, Forterre Y (2002) Friction law for dense granular flows: application to the motion of a mass down a rough inclined plane. J Fluid Mech 453:133–151

Pudasaini SP, Hutter K (2006) Avalanche dynamics: dynamics of rapid flows of dense granular avalanches. Springer, Berlin

Samaniego P, Yepes H, Arellano S, Palacios P, Mothes P, Le Pennec JL, Troncoso L, IG-EPN staff (2007) Monitoring a waxing and waning volcanic activity: the July 14th and August 16th 2006 eruptions of Tungurahua volcano (Ecuador). Cities on Volcanoes 5, Shimabara, Japan

Saucedo R, Macias JL, Sheridan MF, Bursik MI, Komorowski JC (2005) Modeling of pyroclastic flows of Colima Volcano, Mexico: implications for hazard assessment. J Volcanol Geotherm Res 139:103–115

Savage SB, Hutter K (1989) The motion of a finite mass of granular material down a rough incline. J Fluid Mech 199:177–215

Savage SB, Hutter K (1991) The dynamics of avalanches of granular materials from initiation to runout. Part I: analysis. Acta Mech 86:201–223

Sheridan MF (1979) Emplacement of pyroclastic flows: a review. Sp Paper Geol Soc Amer 180:125–136

Sparks RSJ (1976) Grain size variations in ignimbrites and implications for the transport of pyroclastic flows. Sedimentology 23:147–188

Wadge G, Jackson P, Bower SM, Woods AW, Calder E (1998) Computer simulations of pyroclastic flows from dome collapse. Geophys Res Lett 25(19):3677–3680

Yamamoto T, Takarada S, Suto S (1993) Pyroclastic flows from the 1991 eruption of Unzen volcano, Japan. Bull Volcanol 55:166–175